Production, characterization and modelling of WC-Cu cermets

Rita Fonseca Faustino

rita.faustino@tecnico.ulisboa.pt

Abstract

Copper-matrix composites reinforced with tungsten carbide have been studied for application as transition layer in the divertor of nuclear fusion reactors. Composites with 25, 50 and 75% by volume of WC and the remain in Cu have been produced by the hot-pressing sintering method. Three types of samples were produced: (i) mixture of two particle sizes of WC (1+18 μm, bimodal distribution), (ii) particles of WC coated with a Cu layer using sputtering technique (18 μm, monomodal distribution) and (iii) a multi-layer system with gradual composition in WC (1 μm, monomodal distribution). The relative density, thermal diffusivity and hardness of the consolidated materials were evaluated, and the microstructures were analysed by scanning electron microscopy. The results indicate that composites produced with coated WC particles have higher thermal diffusivity values than those with uncoated particles. Moreover, the presence of Cu coating reduces porosity in the interfacial area between large particles and matrix, improving WC/Cu bonding. However, large particles of WC weaken the mechanical behaviour of the WC-Cu composite. Finally, finite element models were used to analyse the thermal behaviour of a material with the thermal properties of the composite with 75% by volume of WC, with bimodal distribution. The effects of porosity and radiation losses in the thermal response of the material were also analysed. The results show that the location of the pores has a greater influence than their size. Both effects lead to a decrease in the thermal diffusivity.

Keywords: WC-Cu composites, hot pressing, thermal diffusivity, size effect, modelling

1. Introduction

The reliable capability of handling power generated in a fusion reactor was identified as one of the most serious technological and scientific challenges for commercially feasible fusion power station [1]. There is a thermal operation gap existing between the PFC (Plasma facing component), made of tungsten (W), and HSM (heat sink material), composed by CuCrZr, where in the limit, the W armour must operate above the 400ºC, and the CuCrZr structural compound between 150 and 350ºC. A thermal strain mismatch between the armour and structure is also reported [1], induced due to the dissimilar values of coefficient of thermal expansion (CTE) of the referred materials.

Therefore, an interlayer in-between the PFC and the heat sink is necessary to guarantee a gradual thermal transition and redistribution of the heat along this new layer. The purpose of the interlayer would be to alleviate the heat flux by diverting it around the tube through the armour [1, 2], in a way that the maximum temperature in the tube is reduced. For ITER, the chosen interlayer consisted of pure soft-annealed copper. However, its high thermal conductivity does not allow a satisfactory temperature gradient generation between the neighbouring layers [3].

Metal matrix composite (MMC) materials are expected to introduce a gentle transition from the brittle behaviour of W, to the ductile behaviour of CuCrZr, due to their hybrid characteristics as a composite.

Cu matrix composites reinforced with WC, WC-Cu, have been advised as transition layer, since Cu is a good electrical conductor and the composition can be optimized for controls the thermal conductivity. Moreover, tungsten carbide (WC) combines favourable properties, such as high hardness, plasticity and good wettability by molten metals [4, 5].

The present work is focused on the production of WC-Cu cermets (ceramic-metallic composite) with a content of 25, 50 and 75 vol% of WC and the remainder of Cu. cermets were produced with the following features, for each composition:

- Bimodal composition: WC-Cu with two distinct particle sizes of WC (1+18 μm). The volume fraction of WC is constituted by 50% of each specie;
- Monomodal composition: WC-Cu with one particle size of WC (18 μm). For this category, cermets were produced with both coated particles and with non-coated ones. The coat is a Cu 560 nm thick nanolayer, deposited onto the WC particles by D.C. magnetron sputtering deposition;
- Graded composition: WC-Cu with a functional graded composition of the three singular compositions, with WC with one particle size (1 μm). the layers were simplu deposited in top of each other.

WC-Cu cermets were produced by a powder metallurgy process, namely blending and sintering WC and Cu powders by hot-pressing that is simple and low cost. The effectiveness of sintering was analysed by the method of Archimedes and SEM imaging, Phase identification of consolidated specimens and presence of impurities were analysed by X-ray diffraction(XRD), thermal properties were investigated by laser flash technique (LFT) and hardness values were obtained. Finally, FE (finite element) models were developed to simulate the thermal transport behaviour of a tested specimen, where the effect of additional porosity was analysed.

2. Experimental

The raw materials were in powder form. Cu spherical powders were used as the matrix material (average size: 37 µm, purity: >99.9%, Alfa Aesar) and WC particles (average size: 18 and 1 µm, purity: >99.5%, Sigma-Aldrich) as particulate reinforcement, with irregular shape. A share of WC particles was coated with Cu by D.C. magnetron sputtering deposition. The powders were mixed by turbula blending for one hour, after being weighted inside a glove box, to avoid copper oxidation and then submitted to hot pressing in an industrial environment.

The sintering process consisted in heating the material till a temperature varying from 850 to 1150ºC, under pressures from to 22 to 47 MPa, during 15 to 25 minutes, in an Idea Vulcan 70 VP heating furnace. The estimated heating rate is approximately equal to 120 °C/min and is the same for all the cycles, where the specimens were left to cool in the furnace. The powder mixture was consolidated in graphite dies of 55x10x5 mm size. Figure 1 presents the sintering temperature and time, faced to the T_m^{Cu} (Cu melting temperature), as comparison term.

The real density of the produced cermet was obtained by the method of Archimedes. Thermal diffusivity (α) values were measured LFT on the apparatus *FL-5000* from Anter Corporation, for samples with a densification bigger than 95%, due to the porosity negative impact on the α values.

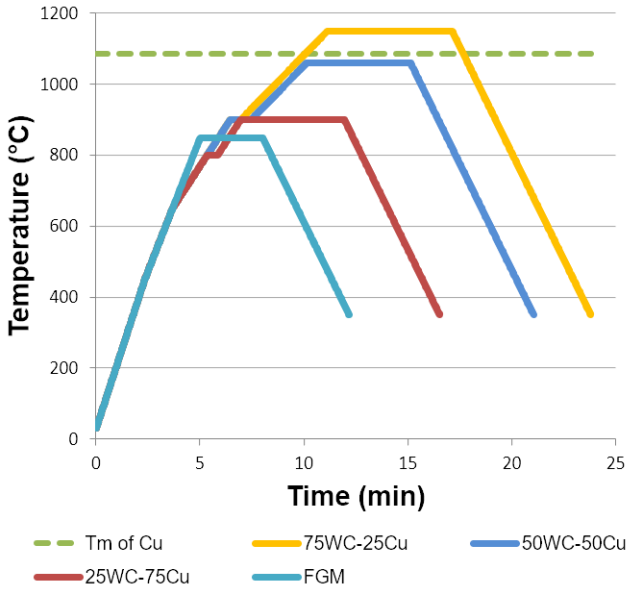

Figure 1 Temperature versus time of sintering of the cermets with compositions of 75WC-25Cu, 50WC-50Cu and 25WC-75Cu in volume percent, with the indication of the melting temperature of Cu. Heating rate of 120 °C/min for the three compositions.

The heat capacity at constant pressure (c_p) was measured for one cermet presenting a density $\geq 95\%$, using modulated differential scanning calorimetry (MDSC), in a Q2000 apparatus, from TA Instruments. α and c_p were obtained for the same temperature range, to obtain the thermal conductivity (k) through the relation $k(T) = \alpha(T)\rho(T)\, c_p(T)$. X-ray diffraction (XRD) measurements were carried out to in a Bruker D8 AXS diffractometer that produces characteristic radiation from an anode made of copper (Cu Kα1 and Kα2 lines). Vickers was measured on a ZHVµ Micro Vickers hardness tester. The test conditions were the applied load of 2 and 20 N and a dwell time of 15 seconds.

3. Results and discussion

Consolidation and microstructure

Knowing that T_m^{Cu} is 1085º C, solid-state sintering should have taken place. However, the copper melted along the production of the samples with a Cu content of 25 vol.%, since it spread out from the graphite mould. The pyrometer measuring the temperature is in contact with the mould and not the sample, so there is an error associated. Also, the melting can be achieved during temperature peaks, in the furnace. XRD revealed no impurities in the WC-Cu system.

Bimodal distribution

Figure 3 shows the micrographs of the produced WC–Cu cermets with 25, 50 and 75 vol% of Cu and the remainder of WC, respectively, having the latter a bimodal size distribution of fine and coarse particles. The two different phases can clearly be distinguished. Furthermore, the microstructures show the matrix material not filling all the void spaces, since porosity is quite visible.

In this composites of 25 and 50vol.% WC, the quantity of small particles was not enough to fill the space left between coarse particles, as shown in Figure 3 (a) and (b).

For the bimodal system, copper infiltrates among fine particles by the capillarity effect, where the liquid that wets the particles generates an interparticle capillary force on grain contacts.

The micrographs in Figure 2 show that the wetting behaviour of Cu on WC is not ideal, allowing some porosity to install on the ceramic-metal interfaces, affecting both the heat and the load transfer from the matrix to the ceramic particles. The filling of the spaces among the bigger particles by the smaller ones is noticeable, for the higher content in WC, leading to a high densification for the sample with the highest WC content.

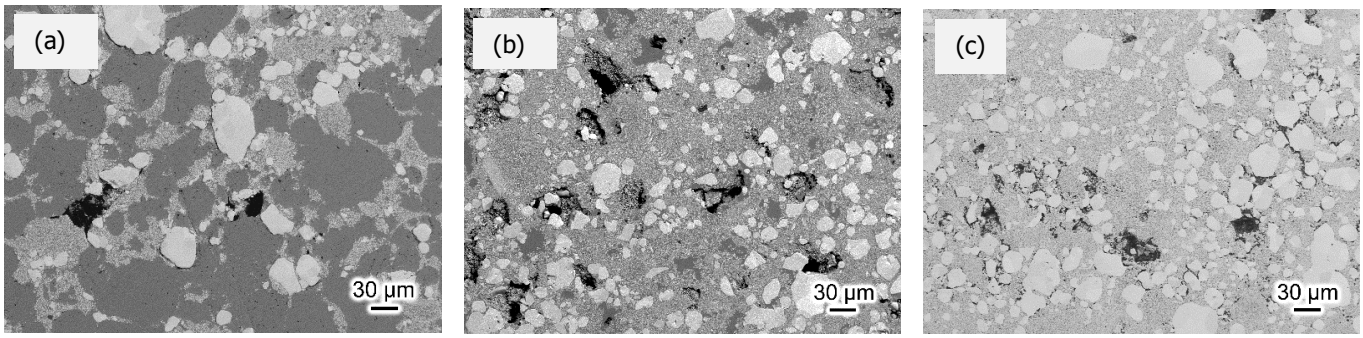

Figure 3 Scanning electron microscopy (SEM) micrographs of WC–Cu cermets with a composition of (a) 25 vol.%WC–75 vol.%Cu, (b) 50 vol.%WC–50 vol.%Cu, and (c) 75 vol.%WC–25 vol.%Cu,

Monomodal distribution

The new strategy to optimize the densification (higher than 95%) is to cover the ceramic particles (WC) with a thin layer of the same material as the matrix one (Cu), attempting to reduce the interfacial energy between matrix and dispersed particles and consequentially, reducing the pores presence, heading to denser samples.

WC particles were covered with Cu by sputtering technology, which is not sensible to particles with an average size less than 10 µm. In this way, the dispersed phase is composed by a monomodal size dispersion of 18 µm, only. Cermets with uncoated 18 µm particles were also synthesized as control samples.

The copper has melted in the three compositions, for both the coated and uncoated samples, concluding that liquid-state sintering took place. Once again, there was copper drainage from the moulds, but it took place for all the specimens except for the sample of 75 vol.% WC with the monomodal uncoated system. Such event could be explained with the use of big sized particles. Due the mutual insolubility in the W-Cu-C system, the capillarity force is the main effect to obtain high densification. However, the capillary effect is more effective for copper infiltration among finer particles and having acute angles [6, 7]. In this way, the use of big particles with roundish surfaces resulted in a decrease of the capillarity effect, leading to copper draining from the mould in all the produced cermets with big sized ceramic particles. This was associated with lack of adhesion of the metal matrix to the particles, due to the non-immediate wetting of WC by Cu.

SEM images of Figure 3 show a more homogeneous structure for the monomodal than for the bimodal composites and also a better adhesion among the two phases.

Graded composition

The consolidation of the composite with a graded composition was a preliminary attempt with the goal of understanding the adhesion of the three layers. The relative density of the produced FGM is of 79%. The three gradient layers were indistinguishable regarding their different composition of 25, 50 and 75 vol% WC. The sintering operation revealed not to be the most indicated, since porosity is mostly located in that diffuse intermediate area. In this way, adding a fine layer of copper might work to bond the two neighbouring layers.

Thermal properties

α was determined only for samples with a densification above 90%. The samples with an adequate level of densification were, for the bimodal size distribution of WC, the 75WC-25Cu, and for the monomodal one, both 25WC-75Cu and 50WC-50Cu with covered WC particles.

The experimental α are indicated in Figure 4. The values are compared to the α of the composing material of the cermets, Cu [8, 9] and WC [10], to the materials of the neighbouring layers in the monoblock, W [11] and CuCrZr [12] and to the WC-Co [13]. As expected, the thermal diffusivity increases with increasing Cu content and the thermal response of the cermet richer is WC is closer to the response of WC and WC-Co. However, the spacing between α, at the same temperature, for the three compositions is not similar, as the cermets compositions might suggest. This must be related to the existence of more interfacial area between matrix and reinforcement for the bimodal system, since in the same volume, smaller particles have more surface area than bigger ones.

Here, the heat flux faces more blocking scenarios: less and thinner copper paths and interception with more particles, which are disposed in a more puzzling way. Meanwhile in the system with coated particles, the presence of large copper regions throughout the microstructure (see Figure 3(b)), works as heat flux "high-ways", easing the heat propagation. Between the two submitted monomodal cermets, the higher copper 50WC_mono. WC–Cu composites show a considerably inferior thermal diffusivity compared to pure CuCrZr and content of the 25WC_mono ensures an even smoother heat flux, comparing to the W. The values of α @ T=145º C is $0.3(\alpha_{bi}) < 0.5(\alpha_{mono}) < 0.7(\alpha_{W}) < 0.9(\alpha_{CuCrZr})\ cm^2.s^{-1}$.

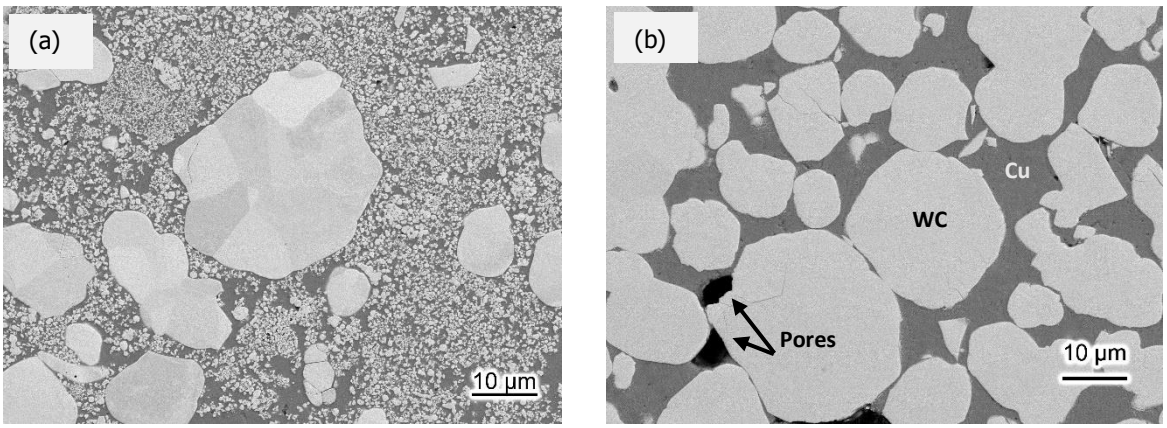

Figure 3 SEM micrographs of WC–Cu cermets with a (a) bimodal composition and a (b) monomodal composition of the reinforcing phase; the cermets have both a composition of 50 vol.%WC–50 vol.%Cu

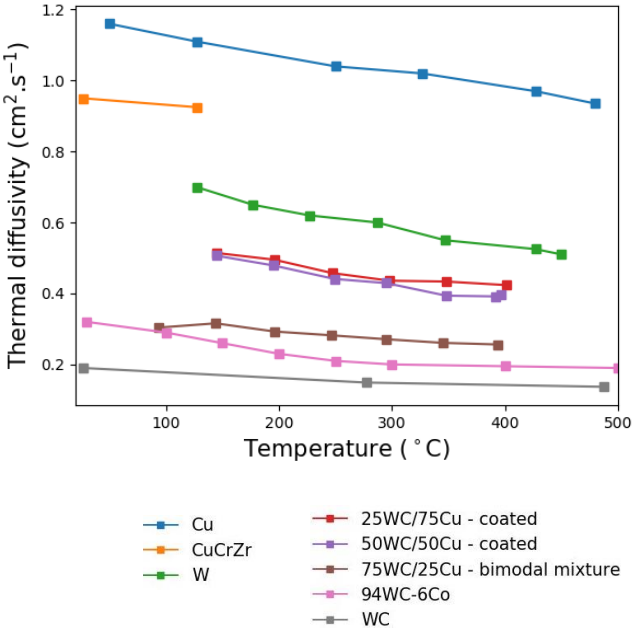

Figure 4 Thermal diffusivity in function of the temperature for Cu [6],[7], CuCrZr [10], W [9], 25 and 50_WC_mono coated, 75WC_bi, WC-Co [11] and WC [8]

Vickers hardness

Figure 5 shows Vickers hardness values of the cermets with bimodal and monomodal size distribution, coated or uncoated. This measurement was not proceeded for the poorly consolidated samples (only >75%), since their pores size would be of a similar order as the indentation depth, compromising the general hardness measured.

The considered values reflect the hardness of the composites, since the material was indented in representative zones.

As expected, increasing WC content yields higher hardness values. Comparing the bimodal with the monomodal cermets with the same volume composition, the bimodal system displays higher hardness values for the three compositional variations. Such increase may be due to the stronger pinning effect of reinforcing particles [14], that bear high loads and whose presence obstruct the movement of dislocations, increasing the hardness. It is also related to the wider dispersion on the base material. As the particles distance more from each other in the bimodal system, they hinder the plastic deformation of the overall material in a greater way, comparing to the system having fewer and bigger particles.More interfaces with pores must result in broader hardness values due to the smaller solid volume which is easier to plastically deform. This is reflected in a wider standard deviation, noticed in the hardness values of 75 vol.% WC with the monomodal uncoated system, which is the less dense material.

4. Modelling

A representative model of a WC-Cu cermet was done, with the aim of describing the transient thermal behaviour of this material using finite element method (FEM).

The temperature-time (TT) response on the rear side of the sample, to obtain thermal diffusivity values.

LFT is one of the experimental methods that returns the time evolution of the temperature. Here, a short laser pulse irradiates the front surface of a sample with a disk format [15], that is adiabatically insulated. Therefore, a computational representation of the laser flash method was developed to study the thermal transport in the synthetized material. The effects of adding porosity and radiation emission in the TT behaviour of the mentioned material are also studied, since these are two features that affect the thermal response.

The study is divided in four sections, which are the following:

1. Adapting the experimental TT data obtained from LFT to the analytical curve behaviour;
2. Developing a standard modelling curve with the parameters used in LFT;
3. Comparison the previous curve with LFT experimental results (point 2), represented by the experimental curve (in point 1). In this step, the simulation conditions are adjusted in order to fit the experimental results. As a result, a set of modelling conditions are obtained, that represent well the behaviour of the tested materials.

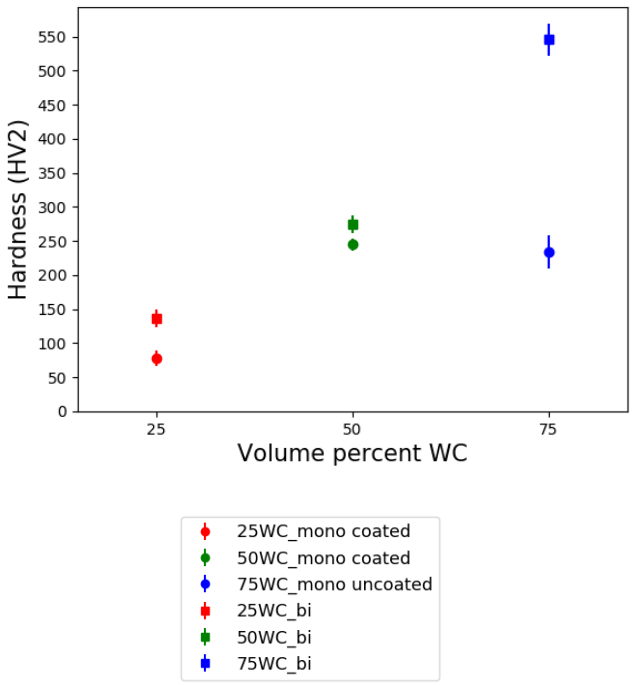

Figure 5 Hardness values of well consolidated cermets as a function of composition in vol% WC

4. Study of the influence of porosity effects on the behaviour of the curve. These results allow to understand the importance of this effects on real materials.

Previously, the space and time algorithms were adapted to best fit the models developed for this work simulation and the resulting TT curve have shown the typical behaviour of the analytical expression, given by

$$\Delta T(L,t) = \frac{Q}{\rho C_p A_c L}\left[1 + 2\sum_{n=1}^{\infty}(-1)^n exp\left(\frac{-n^2\pi^2\alpha t}{L^2}\right)\right] \quad (1)$$

where Q is the energy emitted by the laser pulse onto the superficial area, A_c, of the sample, which has a total thickness L and ρ, C_p and α are the density, specific heat and thermal diffusivity of the sample's material. For the modelling work the studied sample was the sample with 75 vol.% of WC, with bimodal size distribution of the reinforcing phase.

α is directly related to the half-rise time, $t_{0,5}$, that is obtained through a dimensionless temperature-time equation given by

$$V(\omega) = 1 + 2\sum_{n=1}^{\infty}(-1)^n exp\,(-n^2\omega) \quad (2)$$

where

$$V(L,t) = \frac{\Delta T(L,t)}{Q/\rho C_p A_c L} = \frac{\Delta T(L,t)}{\Delta T_{L,max}} \quad (3)$$

$$\omega = \pi^2 \alpha t / L^2 \quad (4)$$

so

$$\omega_{1/2} = 1.37 \leftrightarrow \frac{\pi^2 \alpha t_{0,5}}{L^2} = 1.37 \quad (5)$$

which give a direct relation between α and $t_{1/2}$

$$\alpha = 0.1388\frac{L^2}{t_{0,5}} \quad (6)$$

$K = 0.1388$ is the corresponding value for a 50% rise of T (L,max) [15, 16]. Other constants correspond to other percent rises.

Experimental curve

The fitting of the analytical curve to the experimental points obtained by LFT is done by an optimization algorithm from the Scipy library of Python. This algorithm starts from educated guesses of the fitting parameters. For the first fit, a value of $t_{1/2}$ was considered as initial guess. The latter was extrapolated from the input TT data.

Both the experimental results and the analytical fitting curve are shown in Figure 6 (a). Here is noticeable that the fit is not the best, since a displacement in the edges

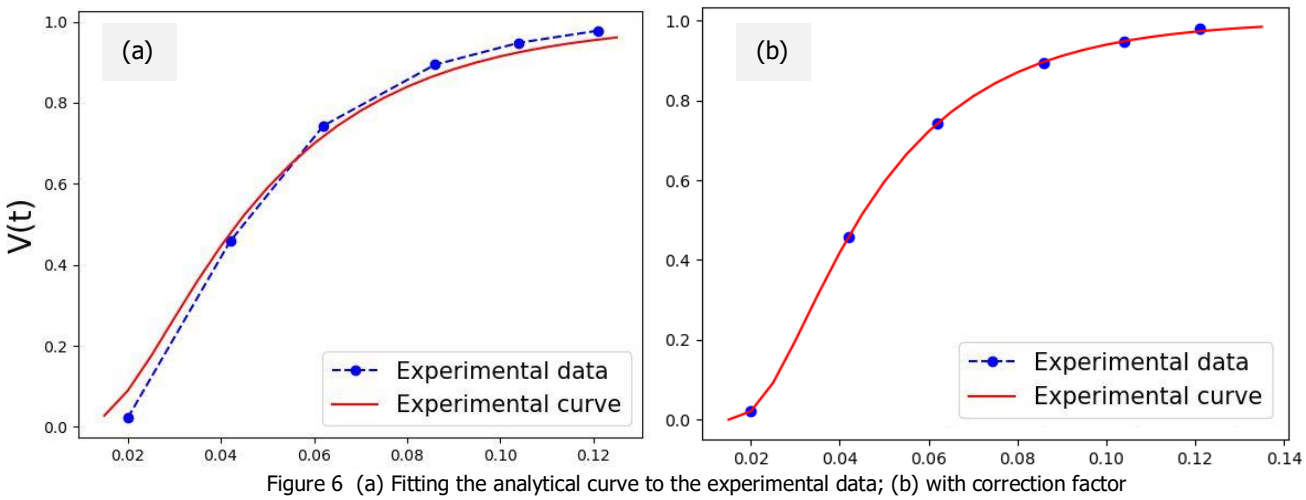

Figure 6 (a) Fitting the analytical curve to the experimental data; (b) with correction factor

is observed. Based on this first results, a second parameter is included, that represents a shift on the time

scale which is another parameter that needs an initial guess to be optimized. The initial miss-fit in Figure 6(a) suggests the possibility of a time difference between the temporal evolutions of the temperature of the sample and the temperature recorded by the apparatus. In this way, an increment (∂t) is added to the time factor in the analytical equation (16), where $t \to t + \delta t$. This implies the exponential argument to be

$$\exp(x) \leftrightarrow x = \frac{-0.1388.n^2\pi^2(t+\partial t)}{t_{0,5}} \qquad (7)$$

For the δt, the initial guess is 0, to consider that no time displacement has really occurred. The returned optimum value for the latter is of -0.0075, suggesting that the measured temperature by the thermocouple is delayed by 0.0075 s (7,5 ms), regarding the time that is set by the apparatus. With this correction, the coefficient of determination (R^2) is 0.9999, proving to be a good fit. The change is noticeable in Figure 6(b), where a perfect overlap is obtained. The latter seems to be a good representation of the experimental data. Comparing the experimental result of α obtained by LFT at $T_i = 667\ K$ and the one resulting from the fitting curve:

- $\alpha_{exp} = 2{,}562 \times 10^{-5} \pm 0{,}028 \times 10^{-5}\ m^2.s^{-1}$
- $\alpha_{comput} = 0.1388\frac{L^2}{t_{1/2}} = 0.1388\frac{(2{,}5\times10^{-3})^2}{0.03383} = 2{,}56 \times 10^{-5}\ m^2.s^{-1}$

This implies that the curve in (b) is an an accurate representation of the experimental data, addressed as *experimental curve*.

Standard modelling curve

The simulation conditions for the 3D model originated the average thermal behaviour showed in Figure 7, for 2D slab and the 3D disk models. The curves perfectly overlap, meaning that the 2D model can be used for forward analysis, addressed as *dense model curve*. Next is analysed if this curve represents the experimental curve with accuracy.

There are three dense model curves due to the uncertainty associated to the obtained value of $\bar{k}$ of the body material, where they correspond to $\bar{k} + error, \bar{k}$ and $\bar{k} - error$. The value for thermal conductivity of the considered material is $k = 83{,}7 \pm 5{,}0$ W.m^{-1}.K^{-1}. The average modelling curve seems to successfully overlap the experimental curve. Its corresponding $t_{1/2}$ is 0,03379 s, giving $\alpha = 2{,}567 \times 10^{-5}\ m^2.s^{-1}$, so the average dense model curve can be used for future thermal studies of the present material.

Porosity effect

After an accurate model is obtained for the 75WC_bi, the effect of porosity is analysed. This can be easily done by introducing a second material to library of materials and to the mesh file, that will be air.

Homogeneously dispersed squared pores with big, medium and smell sizes in a matrix of WC-Cu cermet are modelled, covering 5% of the total area. The corresponding meshes are in Figure 8.

Table 1 presents the resulting α values of the three porous structures, and of the dense material. Values of α for the medium and small pores system show the same result, whereas for the big pores case, the average value of α decreases. The thermal diffusivities of the porous system are lower than the dense one, as expected. Adding pores offers more resistance to the heat flux, since the pores material is air, having a thermal conductivity with three orders of magnitude smaller than the matrix (10^{1} vs 10^{-2}).

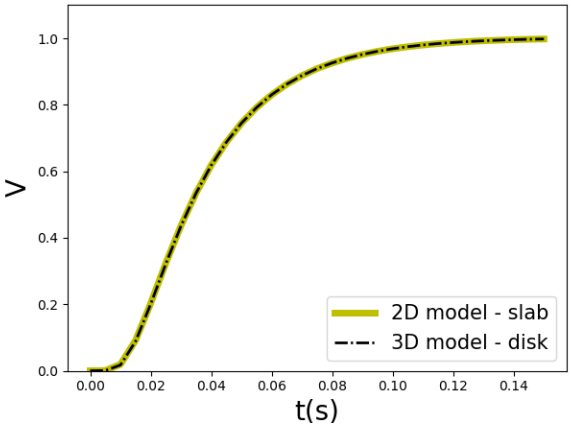

Figure 7 Modelling curves for 2D and 3D models

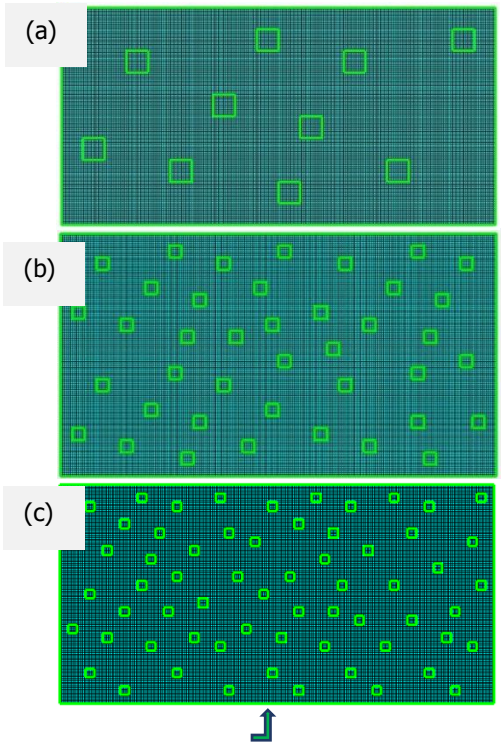

Figure 8 Modelled part with (a) 10 pores, (b) 40 pores and (c) 63 pores with the indication of the measurement point of T in the rear face

The similar values of α for the small and big pores system might be related to the similar distance at which the first pores are located from the surface, represented in Figure 9.

The system in the middle has medium sized pores, so, in 1D, the heat flux travels a bigger distance through pores material than in the small pores system. However, the first pore is the closest to the surface comparing to the one in the small pores system ($\Delta\ell_m < \Delta\ell_s$). Hence, one effect seems to compensate the other and the resulting thermal diffusivity does not vary. In conclusion, the distance in the direction of the heat flux between the surface and pores has a demarcating effect on temperature rise in the rear face, which is measured in the corresponding latitude indicated by the X mark, in the figures.

Even though $\Delta\ell_b$ is the biggest distance, the heat flux travels through bigger pores, roughly with the double length of the small pores, resulting in the lowest thermal diffusivity value.

Material	$t_{1/2}\ (s)$	$\alpha\ (m^2.s^{-1})$
WC-Cu w/ big pores	0,03594	$2{,}414 \times 10^{-5}$
WC-Cu w/ medium pores	0,03487	$2{,}488 \times 10^{-5}$
WC-Cu w/ small pores	0,03487	$2{,}488 \times 10^{-5}$
Dense WC-Cu	0,03379	$2{,}567 \times 10^{-5}$

Table 1 Half rise times and thermal diffusivity values for dense and porous models

5. Conclusions

The conclusions are divided for the materials and modelling studies.

WC-Cu cermets synthesis

WC–Cu composites show a considerably inferior thermal diffusivity compared to pure CuCrZr and W, in a way that they are good applicants as content of the interlayer in the next divertor to build, if the neighbouring layers will be CuCrZr and W.

Due to insolubility between WC and Cu, only physical bonding occurred in the produced composites. The obtained high densification for some of the specimens, above or equal to 95%, was attributed to the capillary force, in the bimodal system. For the monomodal system, high densification occurred due to the faster wetting of the coated WC particles by the matrix, where the same material constitutes both the coating layer and the matrix. However, the majority of samples did not achieve a densification in that range of values $\geq 95\%$. Cermets with a copper rich composition (25 and 50 vol% WC) struggled to properly consolidate, since copper drained out of the mould, probably due to high pressure application (above 22 MPa) combined with the small quantity of WC particles functioning as pinning points to hold the flow of liquid copper. The same phenomenon was verified for all the materials with monomodal size dispersion of WC uncoated particles and for the coated system with 75 vol% WC. Here the combining effects of the pre-coating of particles, that smooths the contact of the binder with the ceramic particles, with the high applied pressure, might have boosted both the copper migration to the pores and to out of the main structure.

In conclusion, small sized particles allow a broader coverage of the reinforcing phase throughout the specimen, resulting in increased bulk hardness, where

the particles shift instead of fracturing. On the other hand, more particles imply a bigger interfacial area, where the pores tend to allocate.

The bimodal mixture of particles obtained the same or lower densification results comparing to the smaller monomodal particle size (1 μm) produced in the previous work, where the expected would be them to obtain better consolidated materials.

The Cu coating layer revealed to have a significant impact in decreasing the thermal resistance between WC particles and Cu matrix, since it smoothed the contact of the binder with the ceramic particles, where the wetting phenomena must have been much easier. In this way, it hindered the formation of pores at the interface. Moreover, micrographs showed the lower agglomeration of reinforcing particles for the coated system in comparison to both uncoated systems. Particle agglomeration represents a weaker region in the mechanical point of view. There is a size compromise by choosing to coat the particles by sputtering –particles with a larger size than 10 μm must be used, but the use of smaller

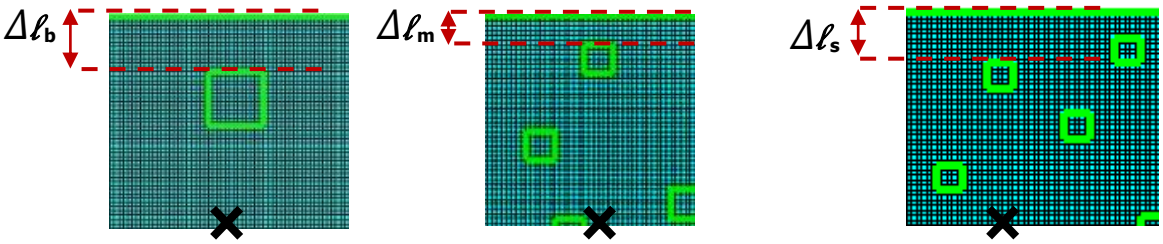

Figure 9 Distance from the upper face to the first pore, aligned to the T measurement point (X mark) for the model with medium (left) and small (right) pores

particles does improve the hardness and the adhesion between matrix and reinforcing phase, since there is more interfacial area in small singular portions (more anchor points), which are desired features.

The composite with a graded composition is at a preliminary state, where three aspects would need to be study, namely the pre-sintering of the three sub-layers, their bonding with a fine layer of copper and also the revision of the sintering parameters. These features are suggested for future work. Also, the sintering maximum pressure of the monomodal system should be revised, since it does not require such that great pressure to achieve consolidation.

Modelling

The thermal behaviour of a WC-Cu cermet was modelled, and simulations were proceeded until the thermal diffusivity and the time-temperature relation were found to be the same of the experimental ones, indicating the best representation of the material by the model. This was achieved, but with a time misfit of 7.5 ms. This time deviation seems to be related to a delay of the measured temperature by the thermocouple in comparison to the beginning of time recording by the apparatus.

The study of the porosity in the current work showed that producing specimens with porosity can be a way of delaying its thermal response, and that their localization is important to this feature.

As future work is suggested the study of the thermal and stress analysis of a complete slab of the monoblock in the divertor, whose outer layer is directly under a thermal load. This should allow the study of structural variations that would lead to a most fitting thermal behaviour for the interlayer, inside the whole monoblock unit, in order to expose the neighbouring layers only at their working temperature ranges.

6. References

[1] J. H. You *et al.*, "European DEMO divertor target: Operational requirements and material-design interface," *Nucl. Mater. Energy*, vol. 0, pp. 1–6, 2015.

[2] T. R. Barrett *et al.*, "Enhancing the DEMO divertor target by interlayer engineering," *Fusion Eng. Des.*, vol. 98–99, pp. 1216–1220, 2015.

[3] D. Hancock *et al.*, "Testing candidate interlayers for an enhanced water-cooled divertor target," *Fusion Eng. Des.*, vol. 98–99, pp. 1323–1327, 2015.

[4] A. Chrysanthou and G. Erbaccio, "Production of copper-matrix composites by in situ processing," *J. Mater. Sci.*, vol. 30, no. 24, pp. 6339–6344, 1995.

[5] V. L. Silva, C. M. Fernandes, and A. M. R. Senos, "Copper wettability on tungsten carbide surfaces," *Ceram. Int.*, vol. 42, no. 1, pp. 1191–1196, 2016.

[6] G. P. Martins, D. L. Olson, and G. R. Edwards, "Modeling of infiltration kinetics for liquid metal processing of composites," *Metall. Trans. B*, vol. 19, no. 1, pp. 95–101, 1988.

[7] A. R. Kennedy, J. D. Wood, and B. M. Weager, "The wetting and spontaneous infiltration of ceramics by molten copper," *J. Mater. Sci.*, vol. 35, no. 12, pp. 2909–2912, 2000.

[8] P. H. Sidles and G. C. Danielson, "Thermal Diffusivity of Metals at High Temperatures," *J. Appl. Phys.*, vol. 25, no. 1, pp. 58–66, 1954.

[9] A. G. P. J. E. Jensen, W. A. Tuttle, R. B. Stewart, H. Brechna, "Section XV," in *Cryogenic Data Notebook*, vol. I, 1980.

[10] M. Akoshima, Y. Yamashita, Y. Hishinuma, T. Tanaka, and T. Muroga, "Thermal Diffusivity Measurements of Candidate Ceramic Materials for Shielding Blankets," *ECTP2014 - 20th European Conference on Thermophysical Properties*. 2014.

[11] M. Fujitsuka, B. Tsuchiya, I. Mutoh, T. Tanabe, and T. Shikama, "Effect of neutron irradiation on thermal diffusivity of tungsten-rhenium alloys," *J. Nucl. Mater.*, vol. 283–287, pp. 1148–1151, 2000.

[12] T. B. M. Rohde, F. Hemberger, "Intercomparison of thermal diffusivity measurements on CuCrZr and PMMA," *High Temp. Press.*, vol. 42, no. 6, pp. 469–474, 2013.

[13] P. Miranzo *et al.*, "Thermal conductivity enhancement in cutting tools by chemical vapor deposition diamond coating," *Diam. Relat. Mater.*, vol. 11, pp. 703–707, 2002.

[14] J. Khosravi, M. Givi, M. Barmouz, and A. Rahi, "Microstructural, mechanical, and thermophysical characterization of Cu/WC composite layers fabricated via friction stir processing," *Int. J. Addict. Manuf. Technol.*, vol. 74, no. 5–8, pp. 1087–1096, 2014.

[15] M. a Sheikh, S. C. Taylor, D. R. Hayhurst, and R. Taylor, "Measurement of thermal diffusivity of isotropic materials using a laser flash method and its validation by finite element analysis," *Mater. Sci.*, vol. 33, pp. 1536–1550, 2000.

[16] E. Kaufmann, *Characterization of Materials*, 1st ed. New Jersey: John Wiley & Sons, Inc., 2003.